analytical chemistry

Article

Cite This: Anal. Chem. 2018, 90, 6749−6756

pubs.acs.org/ac

Specific Detection of Proteins Using Exceptionally Responsive Magnetic Particles

Yi-Ting Chen,[†] Riddhiman Medhi,[†] Ivan Nekrashevich,[‡] Dmitri Litvinov,[†,‡] Shoujun Xu,*[,†,§] and T. Randall Lee*[,†,§]

[†]Department of Chemistry, [‡]Department of Electrical and Computer Engineering, and [§]Texas Center for Superconductivity, University of Houston, Houston, Texas 77204, United States

Supporting Information

ABSTRACT: Sensitivity and specificity are among the most important parameters for viable sensor technologies based on magnetic nanoparticles. In this work, we describe synthetic routes and analytical approaches to improve both aspects. Magnetic iron oxide particles having diameters of 120, 440, and 700 nm were synthesized, and their surfaces were specifically functionalized. The larger particles showed significantly stronger magnetic signals and responses when compared to commercially available magnetic particles (Dynabeads). A force-based detection method was used to distinguish specifically bound particles (via protein interactions) and nonspecifically bound ones (e.g., via physisorption). In addition, an exchange platform, denoted as exchange-induced remnant magnetization (EXIRM), was developed and utilized to detect label-free proteins specifically. Using EXIRM, the 700 nm magnetic particles showed a 7-fold increase in detection sensitivity when compared to the markedly larger commercially available Dynabeads; furthermore, EXIRM exhibited high specificity, even in a 100-fold increase of nontargeted protein. More generally, particle size effects, reaction times, and dynamic ranges are evaluated and discussed herein.

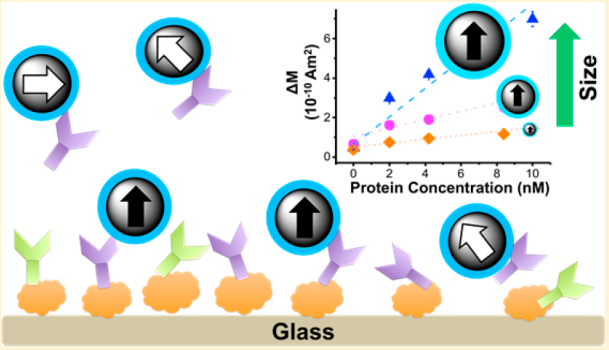

Magnetic particles (MPs) are widely used in protein purification and detection,[1,2] having served as separation tools, target labels, signal carriers, and even force transducers.[1−5] Various detection techniques that utilize MPs have been reported, such as chromatography, surface plasmon resonance, optical/fluorescence spectroscopy, magnetic spectroscopy, and the recently invented force-induced remnant magnetization spectroscopy (FIRMS), which measures the binding forces of protein−protein interactions using magnetic detection.[4,6−8] Derived from the FIRMS technique, the method of exchange-induced remnant magnetization (EXIRM) has been used to study the exchange reaction between microRNA (miRNA) and mismatched DNA.[9] With EXIRM, because the binding between complementary RNA/DNA strands is strongest when there are no mismatching nucleotides, mismatched RNA/DNA labeled with MPs are replaced by complementary strands that are unlabeled, leading to a reduction in the magnetic signal. With this approach, the specific detection of miRNA has been achieved: an atomic magnetometer was used to detect the magnetic signals of functionalized MPs before and after applying mechanical forces to remove the nonspecific interactions.[9]

However, it still remains a challenge to detect proteins specifically and with high sensitivity. First of all, protein−protein interactions are generally more complicated and less resolvable than DNA−DNA interactions. In particular, nonspecific interactions between target proteins and the complementary protein-functionalized surface are a major factor inhibiting the development of MP-based specific protein detection.[10] Second, commercially available MPs are magnetically weak in general, which represents a major factor limiting the sensitivity of MP-based detection techniques. The size of the MPs not only governs the magnetic signal but also plays an important role in partitioning the specific and nonspecific interactions between protein-conjugated MPs and the complementary protein-modified surface.[11,12] Moreover, despite the plethora of synthetic routes for the preparation of MPs having various compositions, sizes, and morphologies,[13−15] most of the existing routes afford small particles or particles that have weak magnetic properties.[14−17]

Herein, we report the highly sensitive and specific detection of proteins using the EXIRM technique. To demonstrate this achievement, this manuscript describes the synthesis and characterization of exceptionally strong MPs, their functionalization with streptavidin, and their application in specific protein detection using EXIRM (see Scheme 1). We prepared three different sizes of iron oxide MPs with fairly narrow distributions, 700 ± 165 nm (MP700), 440 ± 90 nm (MP400),

Received: February 4, 2018
Accepted: May 7, 2018
Published: May 7, 2018

DOI: 10.1021/acs.analchem.8b00593
Anal. Chem. 2018, 90, 6749−6756

Scheme 1. Synthetic Strategy Used to Prepare MPs for Biosensing

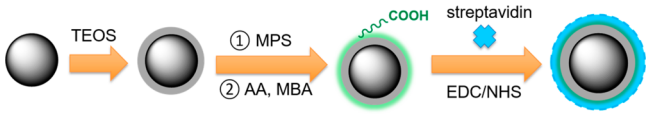

and 120 ± 9 nm (MP100), and functionalized their surfaces for specific protein detection. We compared their magnetic properties to those of widely used and markedly larger Dynabeads (M280, Invitrogen, 2.8 μm diameter). We then used EXIRM to demonstrate the capacity of the synthesized and functionalized MPs for the specific detection of various subclasses of immunoglobulin G (IgG) based on their differing binding affinities with protein A.

EXPERIMENTAL SECTION

Materials. The chemicals, ammonium hydroxide (30% NH_3 in H_2O, EM Science), sodium acetate, ethanol (McKormick Distilling Co.), ethylene glycol (Avator), and iron(III) chloride hexahydrate (Alfa Aesar) were of analytical grade and were used as received. Polyvinylpyrrolidone (PVP, MW ∼55 000 g/mol), *N*-(3-(dimethylamino)propyl)-*N*′-ethylcarbodiimide hydrochloride ($C_8H_{17}N_3$·HCl, EDC), *N*-hydroxysuccinimide ($C_4H_5NO_3$, NHS), streptavidin, mouse IgG2a, glutaraldehyde, phosphate-buffered silane (PBS) buffer, bovine serum albumin (BSA), glycine (NH_2CH_2COOH), tetraethylorthosilicate (TEOS), γ-methacryloxypropyltrimethoxysilane (MPS), acrylic acid (AA), *N*,*N*′-methylenebis(acrylamide) (MBA), acetonitrile, 2,2′-azobis(2-methylpropionitrile) (AIBN), Tween 20, and polyethylene glycol (MW ∼400 g/mol) were used as received from Sigma-Aldrich. Dynabeads-M280 streptavidin, protein A, and biotinylated mouse IgG1 from Thermo Fisher, and biotin-PEG-succinimidyl valerate (MW ∼5000) and m-PEG-succinimidyl valerate (MW ∼5000) from Laysan Bio were also used without modification. DEVCON Clear 2 Ton Epoxy glue was used for the assembly of the functionalized glass wells. Water was purified to a resistivity of 18 MΩ·cm (Academic Milli-Q Water System, Millipore Corporation) and filtered through a 0.22-μm filter membrane to remove any impurities. All glassware and equipment were cleaned in aqua regia and rinsed with Milli-Q water prior to use. Details of all synthetic procedures are provided in the Supporting Information.

Preparation of Fe_3O_4 Particles with 120, 400, and 700 nm Diameters. The general procedure for the synthesis of Fe_3O_4 MPs follows a modification of a procedure reported by Deng et al. and Rittikulsittichai et al.[18,19] In general, this synthesis route involves a liquid reduction reaction between iron chloride ($FeCl_3$) and the solvent (ethylene glycol and diethylene glycol) together with hydrothermal and polyol processes; sodium acetate and polyethylene glycol provide electrostatic stabilization and prevent agglomeration. To achieve tunable sizes with controllable size distributions, many factors need precise control, including the coordinating ligand, the solvent system, the concentration of iron source, and the reaction time.[20−22] The growth of magnetic particles starts from the formation of primary nanocrystals and then agglomeration of secondary structures.

The size of the Fe_3O_4 particles can be well controlled to 20−200 nm using an ethylene glycol (EG)/diethylene glycol (DEG) binary solvent system.[20,23] The bulkier, trivalent, and higher boiling point of DEG coordinates with the iron ion to slow down the agglomeration of Fe_3O_4 primary grains and increase the number of agglomeration centers.[21,23] When the desired size is greater than 200 nm for the MP, EG provides a higher capability for reduction and provides better control of the morphology during the hydrothermal synthesis. Moreover, the concentration of the iron source and the reaction time can be adjusted to grow even larger particles.

To produce a uniform silica shell on the MPs, we used a modification of the sol−gel procedure reported by Stöber et al.[24] This method starts with the hydrolysis of TEOS under basic conditions (e.g., aqueous ammonium hydroxide solution), followed by the condensation and polymerization of TEOS into a silica shell on the surface of the magnetic core. The coating thickness can be controlled by adjusting the relative concentrations of ammonium hydroxide, TEOS, and water. For our experiments, details of the chemicals and descriptions of the procedures used are provided in the Supporting Information. Poly(acrylic) acid-coated MPs (Fe_3O_4@SiO_2@PAA) were prepared via distillation−precipitation polymerization.[25,26] Fe_3O_4@SiO_2 particles were conjugated with the vinyl-terminated silane compound, γ-methacryloxypropyltrimethoxysilane (MPS), to expose olefinic bonds on the surface. The procedure involved the treatment of Fe_3O_4@SiO_2 with NH_4OH and MPS in ethanol. The solution containing the well-dispersed, carboxylic acid-functionalized particles was mixed with EDC and NHS to activate the carboxyl group on the surface for conjugation with streptavidin. As noted above, the details of all synthetic procedures are provided in the Supporting Information.

Characterization of Synthesized MPs. The morphology of the synthesized MPs was evaluated using a LEO-1525 scanning electron microscope (SEM) operating at an accelerating voltage of 15 kV; in these analyses, the MPs were deposited from solution and allowed to dry on a silicon wafer. For characterization of the particle sizes, dynamic light scattering (DLS) measurements were obtained using a Zetasizer Nano ZS (Malvern Instruments) equipped with a He−Ne laser operating at 633 nm. The concentrations of the particles were determined at room temperature at dilute sample concentrations (controlled mass) in deionized water using a NanoSight NS300 (Malvern) with programmable Nanoparticle Tracking Analysis (NTA) software. Each measurement was repeated three times.

Additional characterization was obtained by powder X-ray diffraction (XRD, Siemens, model D5000 X-ray diffractometer). A concentrated sample of the bare Fe_3O_4 particles in water was deposited on a piranha-cleaned glass slide, and XRD data were obtained using Cu Kα radiation over the 2θ range of 0−110°. For characterization of the functionalized particles, X-ray photoelectron spectrometry (XPS) measurements were performed using a PHI 5700 X-ray photoelectron spectrometer equipped with a monochromatic Al Kα X-ray source. For these measurements, the particles were dispersed in water, deposited on a copper-taped silicon wafer, and allowed to dry. Fourier transform infrared spectra (FT-IR) were obtained on dried samples mixed with KBr and compressed to form pellets. All spectra were collected over the range from 800 to 4000 cm^{-1} using a Nexus-670 E.S.P. FT-IR spectrometer. Transmission electron microscope (TEM) imaging was used to analyze the nanoparticles after functionalization using a FEI FP 5018/40 Technai G^2 Spirit BioTWIN instrument equipped with a Gatan Orius CCD camera controller operated at 100 kV. All TEM samples were prepared on 300 mesh holey carbon-coated

DOI: 10.1021/acs.analchem.8b00593
Anal. Chem. 2018, 90, 6749−6756

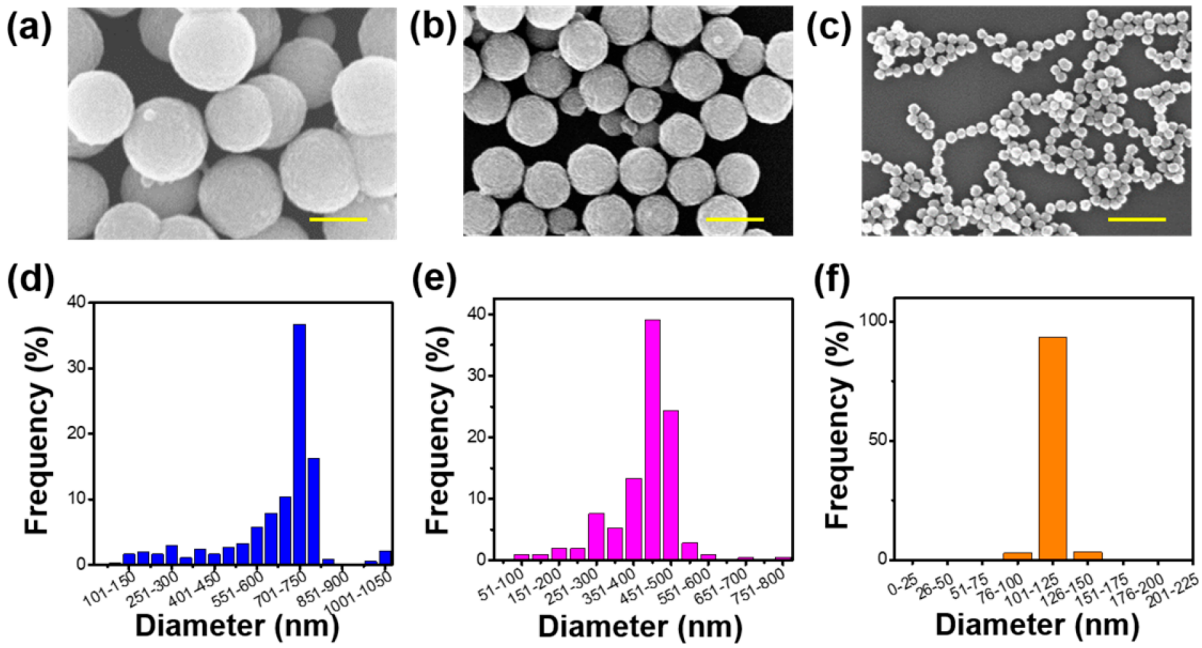

Figure 1. Morphologies and size distributions of the synthesized iron oxide MPs. (a–c) SEM images of MP700, MP400, and MP100, respectively. Scale bar: 500 nm. (d–f) Respective size distributions extracted from the images for MP700, MP400, and MP100.

copper grids and dried before analysis. Thermogravimetric analysis (TGA) measurements were collected using a TA Instruments TGA-2050 under a constant flow of nitrogen (100 mL/min). The temperature was increased from room temperature (25 °C) to 800 °C at a rate of 5 °C/min. Weight measurements were recorded with an accuracy of <±0.3%.

The magnetic properties were obtained using a vibrating sample magnetometer (VSM), LakeShore, model VSM 7300 series with a LakeShore model 735 Controller and LakeShore model 450 Gmeter Software, version 3.8.0, with a known mass of the sample. The atomic magnetometry measurements were obtained using a home-built apparatus with a typical noise level of 1–2 pT during measurements.[27]

Preparation of Biotinylated Substrates and Protein Surfaces. Before functionalization with the amino-terminated silane, (3-aminopropyl)triethoxysilane (APTES), all glass slides were cleaned with acetone, sonicated in 10 M potassium hydroxide solution, and then rinsed with methanol sequentially. The cleaned glass slides were dried by nitrogen gas and kept in the oven at 300 °C overnight. The cleaned and dried glass slides were treated with a methanolic solution containing a 10:1:2 ratio of water:acetate acid:APTES for at least 30 min under sonication. After coating with APTES, the glass slides were dried with nitrogen gas and kept in a desiccator.

Biotin-coated slides were prepared by treatment with a mixture of biotin-PEG-succinimidyl valerate and mPEG-succinimidyl valerate. The active groups (i.e., the succinimidyl-terminated ligands) were coupled to the amino groups on the surface prepared above. Each amino-functionalized slide was incubated with a mixture containing 1.0 mg of biotin-PEG, 6.25 mg of mPEG, and 25 μL of 8.4 mg/mL $NaHCO_3$ for 3 h in the dark. After biotinylation, all slides were rinsed with water and dried with nitrogen gas. A sample well was assembled by gluing the amino-functionalized glass to a 20 × 3 × 1 mm^3 ($L \times W \times H$) piece of polystyrene having a 4 mm × 2 mm oval opening at the center (area ~7 mm^2). Prior to bioconjugation, the sample wells were rinsed with water followed by PBS buffer and then dried with a stream of nitrogen. A streptavidin surface was prepared via conjugation between the biotin-modified surface and streptavidin. The procedure involved the addition of 8 μL of 0.625 mg/mL streptavidin into the biotinylated surface-glued sample well followed by incubation for 1 h.

Protein A slides were prepared by glutaraldehyde cross-linking.[28] To the covalently attached protein (i.e., streptavidin) on the glass slide, 10 μL of glutaraldehyde (2.5 v/v %) was added into the sample well and incubated for at least 1 h. Protein A, at a concentration of 1 mg/mL, was incubated with the aldehyde-activated glass sample well for 2 h. After washing with PBS buffer for three cycles, 10 μL of glycine at 25 mM was used to block the unreacted aldehyde groups on the surface.

Applications of MPs in Protein Detection. To study the specific binding of the streptavidin-functionalized MPs to biotinylated surfaces, the functionalized MPs were dispersed in PBS buffer and incubated with the biotinylated surface in the sample well for 2 h. The samples were then magnetized by a permanent magnet of 0.5 T followed by relaxation for 1 h prior to measurements to ensure stable results. A set of baseline measurements of the magnetic response of the sample were collected using the atomic magnetometer. A mechanical force of 16 pN, provided by a centrifuge (Eppendorf 5018R), was then applied to remove nonspecifically bound MPs. Then, the magnetic response of the samples was measured again, which allowed us to determine the quantity of MPs specifically bound via streptavidin–biotin interactions.

For specific protein detection using the MPs, four types of streptavidin-coated MPs including MP700, MP400, MP100, and the commercial Dynabeads-M280 were diluted to various desired concentrations in PBS buffer that contained 0.05% (w/w) Tween 20. Separately, aliquots of a solution of biotinylated IgG1 antibody (0.02 mg/mL, in PBS at pH 8.0) were added to protein A-modified surfaces and kept at 4 °C overnight. After immobilization of biotinylated IgG1, the sample well was incubated with 3% BSA to reduce nonspecific adsorption. The various streptavidin-conjugated MPs were then added to the

DOI: 10.1021/acs.analchem.8b00593
Anal. Chem. 2018, 90, 6749–6756

protein A-modified surfaces and allowed to incubate for 2 h at room temperature. The samples were then magnetized by a permanent magnet of 0.5 T followed by relaxation for 1 h prior to measurements to ensure stable results. After removing the physisorbed MPs from the IgG1 surface, a set of baseline measurements of the magnetic response of the sample was collected using the atomic magnetometer. The exchange reactions were then performed by incubating the sample well with free IgG2a in PBS buffer at 37 °C for 1 h. The magnetic response was measured again after applying a weak centrifugal force (2 pN). Additional details of the sample preparations are described in the Supporting Information.

RESULTS AND DISCUSSION

Synthesis of Strongly Magnetic Fe_3O_4 Nanoparticles. By adjusting the parameters in the liquid reduction method initially reported by Li and co-workers, we were able to synthesize Fe_3O_4 MPs with desired sizes, even those with unusually large dimensions (i.e., 700 nm diameter). The SEM images in Figure 1a–c show spherical MPs with average diameters of 700 nm (CV ~ 23%), 440 nm (CV ~ 20%), and 120 nm (CV ~ 8%), respectively, where CV is the coefficient of variation. These sample sizes are herein denoted as MP700, MP400, and MP100, respectively, for simplicity in description. Figure 1d–f provides the size distribution diagrams obtained from the corresponding SEM images. In addition, measurements by DLS yielded the mean sizes of the particles in solution to be 709, 480, and 160 nm, respectively. Crystalline structures of the material in the particles were determined utilizing powder X-ray diffraction (XRD), which are shown in Figure S1a. The presence of iron oxide on the particle surfaces was confirmed by XPS (see Figure S1b).

To achieve tunable sizes with well-controlled size distributions, many factors need precise control, including coordinating ligand, solvent system, concentration of iron source, and reaction time.[20−22] The growth of magnetic particles starts from the formation of primary nanocrystals and then the agglomeration of secondary structures.[20−22] Larger primary nanocrystals give rise to materials with stronger magnetic properties.[22] Ethylene glycol and diethylene glycol play the roles of reducing agent and solvent, which offers control of the size range below or above 200 nm. However, the concentration of the iron source and the reaction time are the two main factors that influence the growth of large magnetic particles. A high concentration of the iron source gives large MPs; also, long reaction times lead to relatively large particles.[18,21] Short reaction times terminate the growth of the secondary structure, leading to the production of smaller MPs. Therefore, a precisely controlled reaction time is needed to obtain particles with narrow size distributions.

Magnetic Properties of the MPs. The magnetic properties of the MPs were first investigated with a vibrating sample magnetometer (VSM) at 300 K. Figure 2a shows the hysteresis loop of the bare MP700, MP400, and MP100 particles. Extracted from the hysteresis, the saturation magnetization (M_s) values are 87, 84, and 78 emu/g; and coercivity (H_c) values are 72, 73, and 62 Oe, for MP700, MP400, and MP100, respectively. The M_s values of the three different sizes slightly increase with increasing size, which can be attributed to the stronger interaction within the crystal size and the diameter of the sphere.[29] Moreover, large Fe_3O_4 particles (i.e., larger than the critical size of approximately 25 nm) show large coercivity

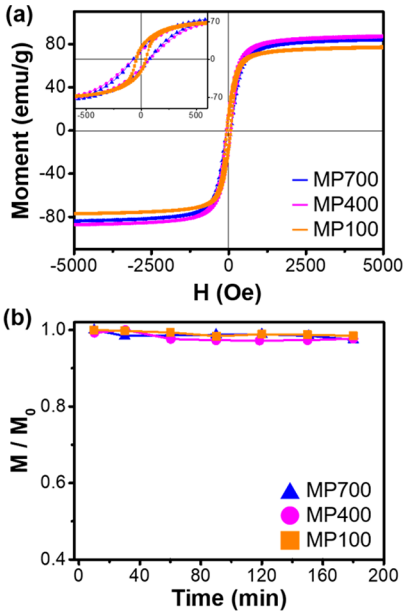

Figure 2. Bulk magnetic properties of the synthesized MPs. (a) Magnetic curves obtained by VSM. Inset provides details of the hysteresis loops and remanent magnetization. (b) Remanent magnetic signal as a function of relaxation time, obtained by an atomic magnetometer.

values due to multidomains of magnetic moments in one large particle.

The remanent magnetization (M_r), which is a key parameter for MP-based biosensing,[12,30,31] can be measured using an atomic magnetometer. Each sample was magnetized for 2 min by a 0.5-T permanent magnet. The M_r for all particles remained constant after 1 h for at least 3 h (Figure 2). It also scaled linearly with the mass of the MPs, as shown in Figure S2a. The stability and linearity of the magnetic signal indicate our MPs are suitable for magnetic detection of proteins using an atomic magnetometer.

To quantify the number of particles in the samples, we used the NanoSight instrument to measure the actual number of MPs in the solution. The principle behind the NanoSight is based on the tracking and counting of individual particles via a video recording of the particles moving under Brownian motion.[32] The measuring range of the NanoSight is 10^7–10^9 particles per mL for iron oxide materials.[32] Figure S2b shows the relationship between the mass concentration and the number concentration of the MPs, which allows us to calculate the number of MPs in a known mass concentration based on the slope obtained from the NanoSight data. The numbers of MPs determined from the NanoSight analysis have a linear relationship with the magnetic response in the atomic magnetometer, as shown in Figure 3a. Consequently, based on those measurements, the magnetization can be quantified for per particle, as shown in Figure 3b.

Notably, the MP700 particle showed a much higher magnetization compared to the smaller MPs (by a factor of 3 compared to MP400 and 46 compared to MP100). In comparison with commercially available M280, the magnetization of a single 2.8 μm M280 is almost half that of MP700. The value is based on the calculation from remanent magnetization and the mass concentration provided by the manufacturer. Therefore, MP700 has the greatest potential to improve the detection sensitivity in biological sensing.

DOI: 10.1021/acs.analchem.8b00593
Anal. Chem. 2018, 90, 6749−6756

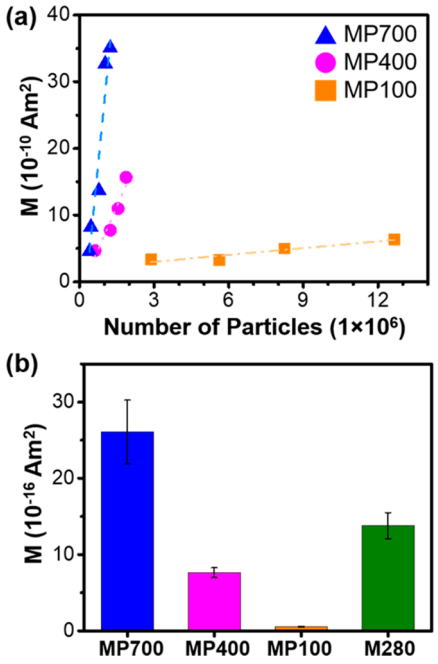

Figure 3. Quantification of single-particle magnetization: (a) quantification of vs number of particles and (b) comparison of the remanent magnetization of synthesized single particles and commercially available M280. M represents the magnetization measured by the magnetometer.

Functionalization of the MPs. For their biological applications, the functionalization of the particles is critical for the stability and their targeted application.[16] To prevent oxidation of the iron oxide surface and to provide biological compatibility, coating the MPs with a silica shell is a commonly used strategy.[13,33,34] In this study, we coated our iron oxide magnetic particles using a modified Stöber method, which offers controlled thicknesses.[24,35,36] The SEM images in Figure 4a–c show silica-coated versions of MP700, MP400, and MP100 with average diameters of 760, 520, and 180 nm, respectively. Using DLS, the mean particle sizes in solution were measured to be 780, 550, and 220 nm, respectively, which are largely consistent with the SEM data. The average thicknesses of the silica shells were therefore approximately 30–40 nm. Analysis by XPS (Figure 4d and Figure S3b) shows a strong peak for Si 2p and no iron Fe 2p peak after coating with silica, which demonstrates that the silica shells completely covered the particles. Additionally, the strong broad band at 1077–1213 cm^{-1} in the IR spectra in Figure 4e, which can be attributed to Si–O–Si stretching, supports the presence of a silica layer.[34,37]

To utilize MPs in biomedical applications, it is often necessary to functionalize their surfaces via conjugation with biological molecules.[38] Carboxyl-functionalized MPs use a well-known carbodiimide coupling method to react with pendant amino groups (e.g., in a protein) to form covalent bonds. After coating the surface with silica, the MPs (Fe_3O_4@SiO_2) were functionalized with a silanizing agent terminated with a polymerizable tailgroup, which was then used to grow a carboxylic acid-terminated polymer layer on the surface of the MPs (see Scheme 1).[36,39] Specifically, before the polymerization process, the MPs were modified with γ-methacryloxypropyltrimethoxysilane to expose reactive vinyl groups; the resultant reactive double bonds on the surface of the particles were used to grow the polymer shell on the surface through distillation precipitation polymerization.[34,40]

The growth of the polymer shell was confirmed and analyzed using TEM (see Figures S4–S6) and also by TGA (see Figure S7). The TEM images of the polymer-coated particles show an increase of the diameter to an average of 820, 560, and 210 nm for samples for MP700, MP400, and MP100, respectively. The average diameter determined by TEM was obtained from at least 20 measurements. From these measurements, we determined that the thickness of the polymer shell is ∼30 nm, ∼20 nm, and ∼15 nm for MP700, MP400, and MP100, respectively. The TGA curves for MP@SiO_2 and MP@SiO_2@PAA are shown in Figure S7. The weight loss observed in the curves of the polymer-coated MPs compared to the SiO_2-coated MPs can be attributed to the decomposition of the

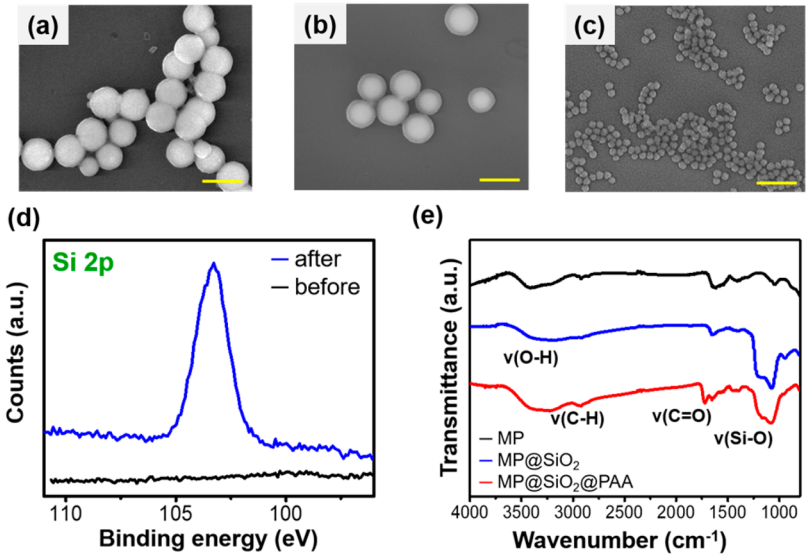

Figure 4. Characterization of the functionalized MPs. (a, b, c) SEM images of the silica-coated MP700, MP400, and MP100, respectively. Scale bar: 1 μm. (d) Elemental characterization of MP700 (both before and after silica coating) by XPS. (e) IR spectra of MP700 throughout the silica-coating process and subsequent functionalization with poly(acrylic) acid (PAA).

DOI: 10.1021/acs.analchem.8b00593
Anal. Chem. 2018, 90, 6749–6756

organic components of the polymer shell. Based on this assumption, the weight residue of the polymer-coated MPs at 800 °C is about 86, 71, and 67 wt %; therefore, we estimate the polymer content to be 7, 20, and 19 wt % in the polymer-functionalized MP700, MP400, and MP100, respectively. Taken together, the TEM and TGA results indicate the successful growth of a thin polymer coating on the MPs.

The presence of carboxylic acid functional groups on the surface of the MPs was confirmed by IR spectroscopy; using MP700 as a representative example, Figure 4e illustrates characteristic peaks of C═O stretching at 1722 and 1652 cm^{-1} for asymmetric and 1435 cm^{-1} for symmetric COO−, and the more obvious C−H stretching vibrations at 2917 cm^{-1}.[34,37,41] As part of the bioconjugation procedure, we modified our carboxylic acid-terminated MPs with streptavidin, which is a common marker to recognize biotinylated biomolecules.[3,5] The TEM images in Figures S4−S6 illustrate the functionalization of the MPs in each step: MP, MP@SiO_2, MP@SiO_2@PAA, and MP@SiO_2@PAA@streptavidin. Figure S8 provides the magnetic characterization (VSM and AM) of the streptavidin-modified MPs.

Applications of the Functionalized Magnetic Nanoparticles. The feasibility of using the streptavidin-conjugated MPs in bioanalytical applications was demonstrated through specific binding with biotinylated surfaces. Due to the substantial nonspecific binding often encountered in particle-based analysis, a unique method of applying a weak mechanical force was used to remove nonspecifically bound MPs. Thus, the remanent magnetization can be attributed to a specific interaction between streptavidin on the MPs and biotin on the surface.

Figure 5 shows the magnetic signals of specific streptavidin−biotin interactions between streptavidin-conjugated MPs and

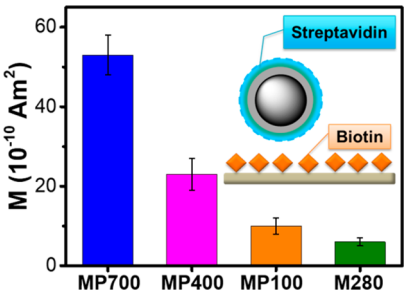

Figure 5. Magnetic signal of streptavidin-conjugated MPs specifically bound to a biotinylated surface.

immobilized biotin. The MP700 particles showed the highest magnetic signal, followed by MP400, MP100, and last M280. When the MPs interact with solid-surface receptors, three factors may affect the overall signal: (1) the magnetization of the individual MPs, (2) the number of MPs bound to the sensing area, and (3) the binding efficacy of the specific ligand−receptor pairs. For a given molecular binding pair, small size and strong magnetic properties will favor signal enhancement. For example, MP700 is both magnetically stronger and physically smaller than M280. Both factors contributed to the 9-fold signal enhancement of MP700 compared to M280. Therefore, our results showed the potential of the synthesized MPs in bioanalytical applications with enhanced sensitivities. In the case of MP100, although the signal is almost two times stronger than M280, their much smaller size will allow *in vivo* applications, whereas M280 is too large for such utilization.

Protein exchange reactions can be demonstrated by taking advantage of the EXIRM technique with surface-based magnetic detection and label-free targets.[9] Detection of a targeted protein in solution, which has higher affinity to the surface-immobilized receptors, can be achieved by replacement of the magnetically labeled protein on the surface. Figure 6a

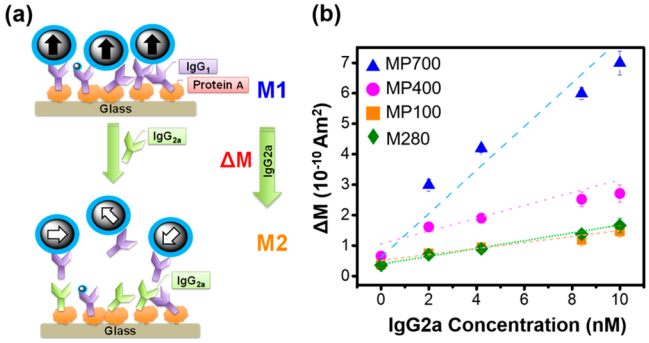

Figure 6. (a) Schematic illustration of the dynamics between the MPs and the surface during analysis by EXIRM. (b) EXIRM data for protein A arising from an exchange between IgG1 and IgG2a subclasses. The magnetic signal decreases with an increase in IgG2a concentration.

illustrates the sample preparation and the principle of the EXIRM experiment. The reaction is based on the different binding affinities of protein A with different subclasses of immunoglobulin IgG; it is well-known that protein A has a strong affinity to mouse IgG2a but a weak affinity to mouse IgG1.[42] Protein A was covalently adsorbed on the glass surface, which was followed by the attachment of biotinylated IgG1. Subsequently, the bound biotinylated IgG1 was labeled with streptavidin-coated MPs. The magnetization was measured after removing nonspecifically bound particles, quantified as M1 in Figure S9. It represents the magnetic response of streptavidin-functionalized MPs bound on the biotinylated IgG1-protein A surface. After introducing IgG2a, the magnetic signal obtained was denoted as M2. ΔM represented the magnetic difference between M1 and M2 (see Figure 6).

Figure 6b shows the results of ΔM when the IgG2a concentration was increased from 2, 4, 8, 10 nM and different MPs were used. All MPs showed good linear responses of ΔM vs [IgG2a] over this range of concentrations. The MP700 particles yielded the largest slope because of their strongest magnetic properties. The MP400 particles showed an intermediate signal change, which was still higher than that of M280. The MP100 particles gave signals that were not significantly different from M280. Regardless of the size difference, the exchange efficiency of 4 nM IgG2a is around 20−23% (calculated by ΔM/M1 × 100%).

The driving force for the exchange reaction can be attributed to the binding affinity difference under our conditions.[42,43] In the control experiment with IgG2a at 0 nM, the samples were incubated with only buffer without IgG2a, and there were no obvious changes in the signal (i.e., ΔM = 0). Additionally, in the control experiment with 100 nM of BSA protein, there were no obvious changes in the magnetic signal. Therefore, the magnetic signal change specifically relates to the intermediacy of IgG2a. Moreover, applying a weak mechanical force can trigger MP dissociation from the surface after the exchange

DOI: 10.1021/acs.analchem.8b00593
Anal. Chem. 2018, 90, 6749−6756

reaction and distinguish specific IgG replacement interactions from nonspecific adsorption.[6]

CONCLUSIONS

We have synthesized MPs with single Fe_3O_4 cores as large as 700 nm. The MPs were successfully functionalized with streptavidin to facilitate biological applications, demonstrated by a wide range of analytical techniques. The combination of size and strong magnetic properties of the synthesized MPs showed sensitivity improvements of 9-, 4-, and 2-fold for MP700, MP400, and MP100, respectively, when compared to the commercial M280 particles. By using the unique exchange method of EXIRM, we demonstrated the specific detection of proteins based on differences in binding affinity; the nonspecific interactions between the MPs and the surface were removed by applying a weak mechanical force. Therefore, by combining strong MPs with the EXIRM method, protein detection can be achieved with both high sensitivity and high specificity.

ASSOCIATED CONTENT

Supporting Information

The Supporting Information is available free of charge on the ACS Publications Web site. Contents include . The Supporting Information is available free of charge on the ACS Publications website at DOI: 10.1021/acs.analchem.8b00593.

Experimental methods, elemental characterization of the magnetic particles, quantification of magnetization per particle, functionalization route, TEM images after each step of the synthetic procedure, TGA analysis of the functionalized magnetic particles, magnetic properties of the functionalized magnetic particles, and magnetic measurements in protein exchange (PDF)

AUTHOR INFORMATION

Corresponding Authors

*E-mail: sxu7@uh.edu.

*E-mail: trlee@uh.edu.

ORCID

Dmitri Litvinov: 0000-0003-2272-562X

T. Randall Lee: 0000-0001-9584-8861

Notes

The authors declare no competing financial interest.

ACKNOWLEDGMENTS

This work was supported by the Air Force Office of Scientific Research (Grant AFOSR FA9550-18-1-0094, T.R.L.), the National Science Foundation (ECCS-1508845, S. X.), and the Robert A. Welch Foundation (E-1320, T.R.L.). T.R.L. and S.X. acknowledge partial support from the Texas Center for Superconductivity at the University of Houston (TcSUH). We would like to thank Dr. Tatyana Makarenko for her help in obtaining the TGA data and Dr. Margaret Gondo from the College of Optometry at the University of Houston for assistance in operating the TEM.

REFERENCES

(1) Yoo, D.; Lee, J.-H.; Shin, T.-H.; Cheon, J. *Acc. Chem. Res.* **2011**, *44*, 863−874.

(2) Lee, H.; Shin, T.-H.; Cheon, J.; Weissleder, R. *Chem. Rev.* **2015**, *115*, 10690−10724.

(3) De Palma, R.; Reekmans, G.; Liu, C.; Wirix-Speetjens, R.; Laureyn, W.; Nilsson, O.; Lagae, L. *Anal. Chem.* **2007**, *79*, 8669−8677.

(4) Yao, L.; Xu, S. *J. Phys. Chem. B* **2012**, *116*, 9944−9948.

(5) Chen, Y.-T.; Jamison, A. C.; Lee, T. R.; Xu, S. *ACS Cent. Sci.* **2016**, *2*, 75−79.

(6) Monson, C. F.; Driscoll, L. N.; Bennion, E.; Miller, C. J.; Majda, M. *Anal. Chem.* **2009**, *81*, 7510−7514.

(7) Chen, C. T.; Chen, C. A.; Tsai, Y. Y.; Yuan, Y. Y.; Huang, Y. C.; Chen, T. S.; Tsai, J. S. C. *IEEE Trans. Magn.* **2014**, *50*, 1−4.

(8) de la Escosura-Muniz, A.; Parolo, C.; Maran, F.; Merkoçi, A. *Nanoscale* **2011**, *3*, 3350−3356.

(9) Yao, L.; Wang, Y.; Xu, S. *Chem. Commun.* **2013**, *49*, 5183−5185.

(10) Hu, Q.; Yang, H.; Wang, Y.; Xu, S. *Chem. Commun.* **2016**, *52*, 3705−3708.

(11) Whitesides, G. M. *Nat. Biotechnol.* **2003**, *21*, 1161−1165.

(12) Yao, L.; Xu, S. *Angew. Chem., Int. Ed.* **2011**, *50*, 4407−4409.

(13) Kolhatkar, A. G.; Nekrashevich, I.; Litvinov, D.; Willson, R. C.; Lee, T. R. *Chem. Mater.* **2013**, *25*, 1092−1097.

(14) Sun, S.; Zeng, H.; Robinson, D. B.; Raoux, S.; Rice, P. M.; Wang, S. X.; Li, G. *J. Am. Chem. Soc.* **2004**, *126*, 273−279.

(15) Santra, S.; Tapec, R.; Theodoropoulou, N.; Dobson, J.; Hebard, A.; Tan, W. *Langmuir* **2001**, *17*, 2900−2906.

(16) Lu, A.-H.; Salabas, E. L.; Schüth, F. *Angew. Chem., Int. Ed.* **2007**, *46*, 1222−1244.

(17) Liu, J.; Qiao, S. Z.; Hu, Q. H.; Lu, G. Q. *Small* **2011**, *7*, 425−443.

(18) Deng, H.; Li, X.; Peng, Q.; Wang, X.; Chen, J.; Li, Y. *Angew. Chem., Int. Ed.* **2005**, *44*, 2782−2785.

(19) Rittikulsittichai, S.; Kolhatkar, A. G.; Sarangi, S.; Vorontsova, M. A.; Vekilov, P. G.; Brazdeikis, A.; Randall Lee, T. *Nanoscale* **2016**, *8*, 11851−11861.

(20) Xuan, S.; Wang, Y.-X. J.; Yu, J. C.; Cham-Fai Leung, K. *Chem. Mater.* **2009**, *21*, 5079−5087.

(21) Yang, X.; Jiang, W.; Liu, L.; Chen, B.; Wu, S.; Sun, D.; Li, F. *J. Magn. Magn. Mater.* **2012**, *324*, 2249−2257.

(22) Ge, J.; Hu, Y.; Biasini, M.; Beyermann, W. P.; Yin, Y. *Angew. Chem., Int. Ed.* **2007**, *46*, 4342−4345.

(23) Xuan, S.; Wang, F.; Wang, Y.-X. J.; Yu, J. C.; Leung, K. C.-F. *J. Mater. Chem.* **2010**, *20*, 5086−5094.

(24) Stöber, W.; Fink, A.; Bohn, E. *J. Colloid Interface Sci.* **1968**, *26*, 62−69.

(25) Fang, C.; Bhattarai, N.; Sun, C.; Zhang, M. *Small* **2009**, *5*, 1637−1641.

(26) Ma, W.; Xu, S.; Li, J.; Guo, J.; Lin, Y.; Wang, C. *J. Polym. Sci., Part A: Polym. Chem.* **2011**, *49*, 2725−2733.

(27) Yao, L.; Xu, S. *Angew. Chem., Int. Ed.* **2009**, *48*, 5679−5682.

(28) Kluchova, K.; Zboril, R.; Tucek, J.; Pecova, M.; Zajoncova, L.; Safarik, I.; Mashlan, M.; Markova, I.; Jancik, D.; Sebela, M.; Bartonkova, H.; Bellesi, V.; Novak, P.; Petridis, D. *Biomaterials* **2009**, *30*, 2855−2863.

(29) Kolhatkar, A.; Jamison, A.; Litvinov, D.; Willson, R.; Lee, T. *Int. J. Mol. Sci.* **2013**, *14*, 15977−16009.

(30) Kotitz, R.; Matz, H.; Trahms, L.; Koch, H.; Weitschies, W.; Rheinlander, T.; Semmler, W.; Bunte, T. *IEEE Trans. Appl. Supercond.* **1997**, *7*, 3678−3681.

(31) Chen, Y.-T.; Kolhatkar, A. G.; Zenasni, O.; Xu, S.; Lee, T. R. *Sensors* **2017**, *17*, 2300.

(32) Hole, P.; Sillence, K.; Hannell, C.; Maguire, C. M.; Roesslein, M.; Suarez, G.; Capracotta, S.; Magdolenova, Z.; Horev-Azaria, L.; Dybowska, A.; Cooke, L.; Haase, A.; Contal, S.; Manø, S.; Vennemann, A.; Sauvain, J.-J.; Staunton, K. C.; Anguissola, S.; Luch, A.; Dusinska, M.; et al. *J. Nanopart. Res.* **2013**, *15*, 2101.

(33) Zhang, C.; Wängler, B.; Morgenstern, B.; Zentgraf, H.; Eisenhut, M.; Untenecker, H.; Krüger, R.; Huss, R.; Seliger, C.; Semmler, W.; Kiessling, F. *Langmuir* **2007**, *23*, 1427−1434.

(34) Li, G.; Zeng, D. L.; Wang, L.; Baoyu; Zong; Neoh, K. G.; Kang, E. T. *Macromolecules* **2009**, *42*, 8561−8565.

(35) Morel, A.-L.; Nikitenko, S. I.; Gionnet, K.; Wattiaux, A.; Lai-Kee-Him, J.; Labrugere, C.; Chevalier, B.; Deleris, G.; Petibois, C.; Brisson, A.; Simonoff, M. *ACS Nano* **2008**, *2*, 847−856.

DOI: 10.1021/acs.analchem.8b00593
Anal. Chem. 2018, 90, 6749−6756

(36) Lu, Y.; Yin, Y.; Mayers, B. T.; Xia, Y. *Nano Lett.* **2002**, *2*, 183−186.
(37) Liu, G.; Yang, X.; Wang, Y. *Polymer* **2007**, *48*, 4385−4392.
(38) Thanh, N. T. K.; Green, L. A. W. *Nano Today* **2010**, *5*, 213−230.
(39) Lin, P.-C.; Chou, P.-H.; Chen, S.-H.; Liao, H.-K.; Wang, K.-Y.; Chen, Y.-J.; Lin, C.-C. *Small* **2006**, *2*, 485−489.
(40) Ma, W.; Zhang, Y.; Li, L.; Zhang, Y.; Yu, M.; Guo, J.; Lu, H.; Wang, C. *Adv. Funct. Mater.* **2013**, *23*, 107−115.
(41) Zhang, Y.; Yang, Y.; Ma, W.; Guo, J.; Lin, Y.; Wang, C. *ACS Appl. Mater. Interfaces* **2013**, *5*, 2626−2633.
(42) Ey, P. L.; Prowse, S. J.; Jenkin, C. R. *Immunochemistry* **1978**, *15*, 429−436.
(43) Dancil, K.-P. S.; Greiner, D. P.; Sailor, M. J. *J. Am. Chem. Soc.* **1999**, *121*, 7925−7930.

DOI: 10.1021/acs.analchem.8b00593
Anal. Chem. 2018, 90, 6749−6756